Hall effect measurements of high-quality Mn_3CuN thin films and the electronic structure

Toshiki Matsumoto,[1] Takafumi Hatano,[1,2,*] Takahiro Urata,[1,2] Kazumasa Iida,[1,2] Koshi Takenaka,[3] and Hiroshi Ikuta[1,2]

[1]*Department of Crystalline Materials Science, Nagoya University, Furo-cho, Chikusa-ku, Nagoya 464-8603, Japan*

[2]*Department of Materials Physics, Nagoya University, Furo-cho, Chikusa-ku, Nagoya 464-8603, Japan*

[3]*Department of Applied Physics, Nagoya University, Furo-cho, Chikusa-ku, Nagoya 464-8603, Japan*

(Received 6 October 2017; revised manuscript received 15 November 2017; published 29 November 2017)

The physical properties of Mn_3CuN were studied using thin films. We found that an annealing process was very effective to improve the film quality, the key of which was the use of Ti that prevented the formation of oxide impurities. Using these high-quality thin films, we found strong strain dependence for the ferromagnetic transition temperature (T_C) and a sign change of the Hall coefficient at T_C. The analysis of Hall coefficient data revealed a sizable decrease of hole concentration and a large increase of electron mobility below T_C, which is discussed in relation to the electronic structure of this material.

DOI: 10.1103/PhysRevB.96.205153

I. INTRODUCTION

Antiperovskite manganese nitrides Mn_3AN (A = transition metal or semiconducting element) exhibit a great variety of magnetic and structural transitions depending on the composition of the A site [1]. This richness of the phase diagram has been attracting a great interest to these compounds, which has further grown with the recent discovery of several intriguing physical properties, such as negative thermal expansion [2,3], large magnetocaloric effect [4], giant magnetostriction [5,6], low-temperature coefficient of resistance [7–9], and giant barocaloric effect [10]. A theoretical discussion has provided a generic picture about the electronic structure of this fascinating compound family, namely, the hybridization of Mn $3d$ and N $2p$ states form narrow subbands with several singularities near the Fermi level [11,12]. Within this picture, the physical properties would sensitively depend on the exact location of the Femi level, which explains the strong composition dependence. However, this model has not been thoroughly tested by experiments. Part of the reason for this is probably the difficulty of crystal growth, since bulk single crystals of antiperovskite manganese nitrides have been obtained only under extreme conditions and are very small [13].

Among the wide material variety, Mn_3CuN is particularly interesting because many of the functionalities mentioned above were discovered with this compound or by partially substituting the Cu site. The pure compound exhibits a large magnetostriction up to 2000 ppm at 9 T below 143 K, where it undergoes a paramagnetic-to-ferromagnetic transition with a simultaneous cubic-to-tetragonal structural deformation [5,7]. This is two orders of magnitude larger than the magnetostriction of ordinal ferromagnetic metals [14], and comparable to the rare-earth-containing compounds used in practical applications, such as $Tb_xDy_{1-x}Fe_2$ (Terfenol-D) [15]. Whereas the fabrication of bulk single crystals has not been reported, there were several attempts to grow thin films of Mn_3CuN. The first study was reported by Sun *et al.*, but the resistivity of their film showed a temperature dependence quite different from that of bulk samples [16]. Difference from bulk samples still existed in a following work by the same group [17], and the authors suggested inaccurate composition, imperfect crystallinity, or strain effect from the substrate as possible origins. Our group fabricated single-phased Mn_3CuN thin films and observed a ferromagnetic transition, but the transition temperature was higher than that of bulk samples, indicating that the quality is still not sufficient [18].

In this paper, we report the fabrication of high-quality single-crystalline Mn_3CuN thin films and the measurements of the physical properties. Although epitaxial thin films were obtained after optimizing the sputtering parameters, the as-grown film was not of sufficient crystalline quality. Therefore, we studied the effect of postgrowth heat treatment, and found that annealing in vacuum was effective in improving the film quality. The temperature dependence of resistivity and magnetization of the obtained Mn_3CuN films showed a behavior similar to bulk samples, and we found that the ferromagnetic transition temperature is strongly strain dependent. We also measured the Hall resistivity and extracted the carrier concentration and mobility. Based on these results, we discuss the electronic structure of Mn_3CuN.

II. EXPERIMENTAL DETAILS

The Mn_3CuN films were fabricated by reactive sputtering using an ultrahigh-field sputtering method that was developed in our group [19,20]. Sputtering was performed in mixed Ar/N_2 gas using a Mn : Cu = 4 : 1 alloy target. The total sputtering pressure P_{total}, the pressure ratio of N_2 to the total gas R_{N2}, the substrate-to-target distance D_{ST}, and the substrate temperature T_S were optimized in a preliminary study, and all the films reported here were prepared with $P_{\text{total}} = 0.176$ Pa, $R_{N2} = 30\%$, $D_{ST} = 160$ mm, and $T_S = 200\,^{\circ}$C. MgO (100) single crystals were used as substrates, and the films were about 90 nm thick. Postgrowth annealing was performed by sealing as-grown films in quartz tubes under vacuum on the order of 10^{-4} Pa. The sealed tube was heated to 650 °C at a rate of 200 °C/h, and furnace cooled to room temperature immediately after reaching the target temperature. X-ray diffraction (XRD) measurements employing Cu-Kα x-ray sources were carried out to check the phase purity, crystal orientation, and the crystallinity of the films, as well as to determine the lattice parameters. The compositions of the thin films were analyzed by electron probe microanalysis (EPMA).

*hatano@mp.pse.nagoya-u.ac.jp

Magnetization was measured using a superconducting quantum interference device magnetometer. Electrical resistivity, magnetoresistance, and Hall resistance were measured using a Physical Property Measurement System (Quantum Design).

III. RESULTS AND DISCUSSION

The black curve in Fig. 1(a) shows the XRD out-of-plane pattern for the as-grown Mn_3CuN thin film. Only the 002 and 004 peaks of the Mn_3CuN phase together with those of the substrate were observed, indicating that the film was single phase and 00*l*-oriented. The out-of-plane lattice parameter was 3.9102 Å, reasonably close to the value of bulk polycrystalline samples, 3.9073 Å [5]. A clear fourfold symmetry was confirmed by the in-plane ϕ scan of the 111 peak as shown in Fig. 1(b), indicating that the film was grown epitaxially. The in-plane alignment was $Mn_3CuN[100] \parallel MgO[100]$. However, the 111 peaks were very broad, implying that the crystallinity was not high.

We next studied the effect of postgrowth annealing in an attempt to improve the film quality. The blue curve in Fig. 1(a) shows the XRD pattern of the film annealed with the process described in Sec. II. Obviously, Mn_3CuN had decomposed and only impurity peaks were observed. Especially notable are the MnO impurity peaks, although the film was annealed in vacuum. We think that a small amount of oxygen might have been entrapped in the film during deposition or was released from the inner wall of the quartz tube during annealing and formed oxide impurities. Therefore, we sealed Ti powders in the quartz tube because Ti is known to act as an oxygen getter. The red curve in Fig. 1(a) shows the XRD pattern of the film thus annealed. As can be seen, no peaks of an oxide impurity were observed and the film was single phase. The in-plane ϕ scan of this film is shown in Fig. 1(b). Clearly, the 111 peaks were much sharper after annealing. We also measured the 002 rocking curves of similarly prepared films. The rocking curve of the as-grown film was very broad with a full width at half maximum value of about 3.2°, which reduced to 1.143° for the film annealed with Ti, indicating a significant improvement in the crystallinity.

Figure 1(c) plots the temperature dependence of resistivity [$\rho(T)$] of the as-grown film and the film annealed with Ti powders. The resistivity of the as-grown film was almost temperature independent. This behavior is similar to the thin film prepared by Na *et al.* [17], but is obviously different from bulk samples, which show a distinct resistivity peak at around 143 K because of structural transition [5,7]. On the other hand, $\rho(T)$ of the annealed film was similar to that of polycrystalline bulk samples.

Although the crystallinity of the films was improved significantly by annealing, there might be a concern of nitrogen deficiency because the film was annealed in vacuum. We therefore checked how the lattice parameters changed with annealing, which are summarized in Table I. As shown in this table, the out-of-plane lattice parameter decreased, while the in-plane one increased by annealing. This is probably because the film adhered more tightly to the substrate after annealing and was strained to match better with the MgO substrate that has a larger lattice parameter than Mn_3CuN. Nevertheless, the volume of the unit cell had barely changed, only increased

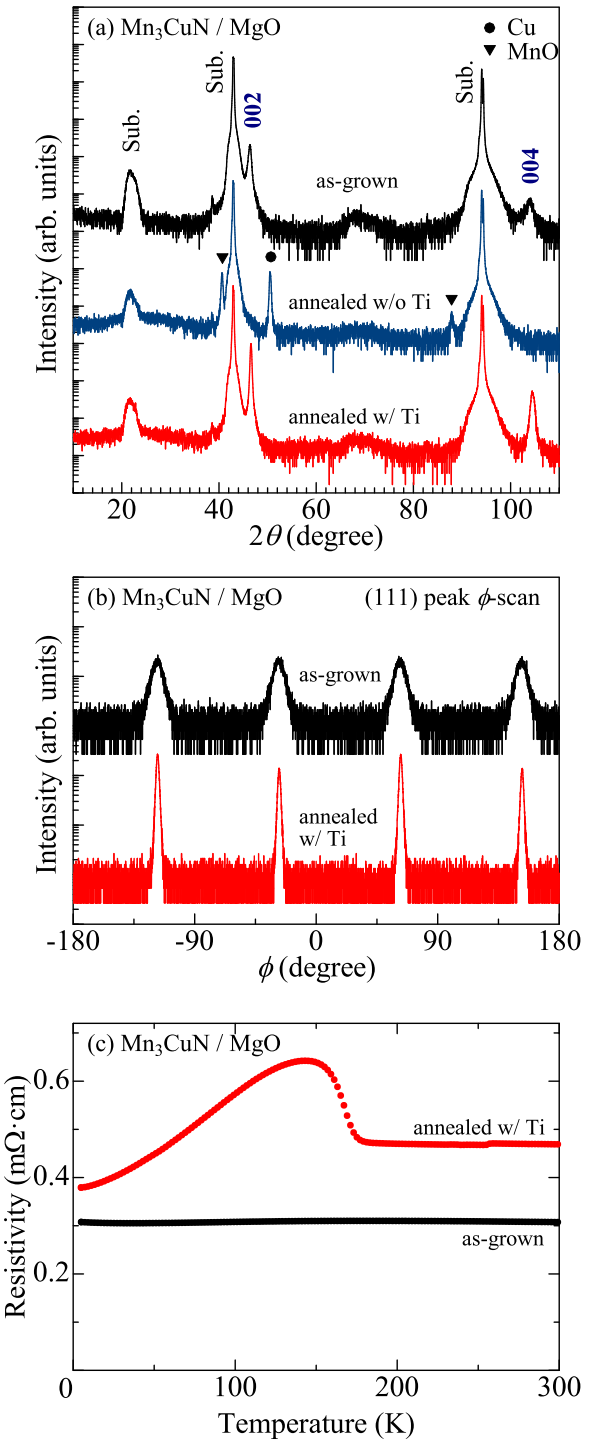

FIG. 1. (a) Out-of-plane XRD patterns of an as-grown Mn_3CuN film, and Mn_3CuN films annealed without and with Ti powders. Impurity peaks corresponding to Cu and MnO are indicated by a solid circle and solid triangles, respectively. (b) 111 peak ϕ-scan XRD patterns and (c) temperature dependence of resistivity of the as-grown film and the film annealed with Ti powders.

slightly (+0.10%). The cell volume of a nitrogen-deficient bulk sample ($Mn_3CuN_{0.8}$) [21] was smaller compared to a sample with almost no nitrogen deficiency prepared by the same group [5]. Further, a related system, $Mn_3Cu_{0.5}Ge_{0.5}N$,

TABLE I. Lattice parameters of Mn_3CuN films at room temperature. The out-of-plane lattice parameters were calculated from the 002 and 004 peaks. The in-plane lattice parameter of the annealed film was calculated from the 200, 220, and 400 peaks measured by grazing-incident XRD, while that of the as-grown film was calculated from the 200 peak only since the other peaks were very weak due to the poorer crystallinity of the as-grown film.

	As-grown	Annealed with Ti
Out-of-plane (Å)	3.9102	3.8956
In-plane (Å)	3.9050	3.9196

also showed a trend of decreasing the cell volume with nitrogen deficiency [22]. Therefore, we think that annealing in vacuum did not affect the nitrogen content of our films notably. Assuming that there is no change in the nitrogen content, the Poisson ratio calculated from the change of the lattice parameters is 0.33.

Figure 2 shows the temperature dependence of magnetization of Mn_3CuN films prepared on different substrates and annealed with Ti powders. For the film grown on MgO, a ferromagnetic transition was observed at 160 K, which is slightly higher than the Curie temperature (T_C) of bulk samples (143 K) [5,7]. It was reported that the magnetic transition shifts to higher temperatures if N is deficient [21] or Mn is excessive [23]. However, in both cases the structural transition temperature (T_{str}), which coincides with T_C in stoichiometric Mn_3CuN, shifts to lower temperature. For nonstoichiometric samples, T_{str} manifests itself in the temperature dependence of magnetization [21,23], but we did not observe the corresponding behavior. Further, the resistivity anomaly that signals the structural transition was observed near T_C [Fig. 1(c)], and the EPMA results gave Mn : Cu = 2.97 : 1.03, reasonably close to stoichiometry. Therefore, it is unlikely that the shift of T_C was caused by N deficiency or Mn excessiveness and we think that it should be attributed to lattice strain. To further explore this possibility, we prepared Mn_3CuN thin films on $MgAl_2O_4$ (100) and $SrTiO_3$ (100) substrates, and measured magnetization (Fig. 2). Obviously, T_C depended on the substrate. In the inset, we plotted T_C as a function of the out-of-plane lattice parameter. Here, we used the bulk value for the lattice parameter of the film grown on $SrTiO_3$, because the XRD peaks of this film overlapped with those of the substrate and it was not possible to separate them due to the almost perfect lattice matching. It is clear from this figure that T_C depends strongly on lattice strain.

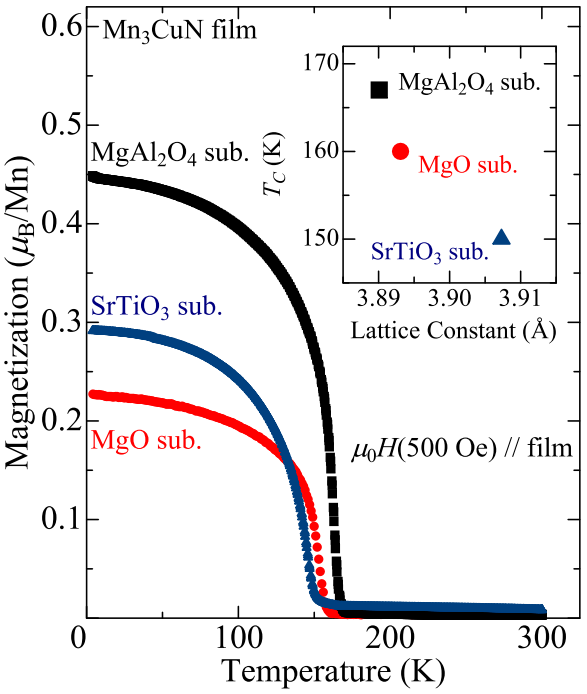

FIG. 2. Temperature dependence of magnetization of Mn_3CuN films prepared on different substrates and annealed with Ti powders. A magnetic field of 500 Oe was applied parallel to the film surface. The inset shows the Curie temperature (T_C) as a function of out-of-plane lattice constant.

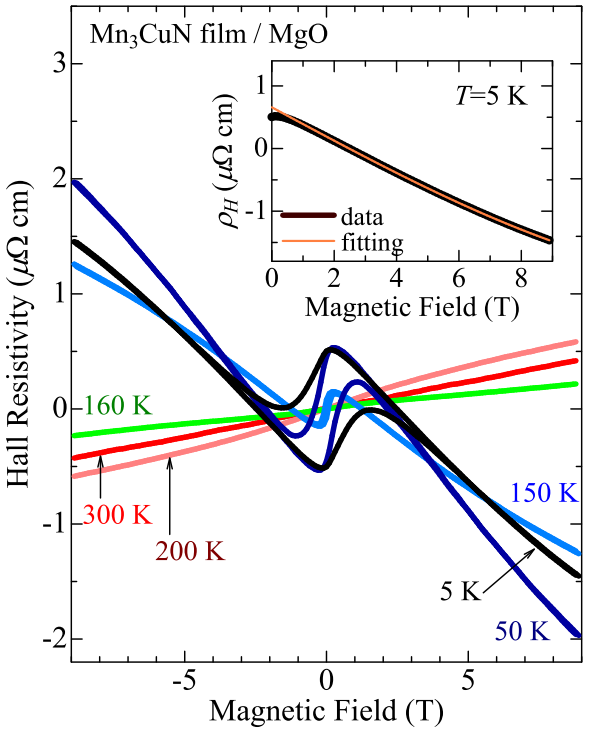

FIG. 3. Magnetic field dependence of Hall resistivity (ρ_H) of the Mn_3CuN film grown on MgO substrate. The inset shows the result of fitting the two-carrier model to the 5 K data at $m_0H \geqslant 5$ T.

Figure 3 shows the magnetic field dependence of Hall resistivity (ρ_H) of the film grown on MgO measured at various temperatures. Obviously, an anomalous Hall effect (AHE) is observed below T_C at low magnetic fields. AHE is commonly observed in ferromagnetic materials, and its microscopic mechanism has gained considerable interest [24,25]. For thin films of Mn_4N, which has the same crystal structure as Mn_3CuN with all Cu replaced by Mn, studies on AHE was reported by two groups [26,27]. It is interesting to note that the anomalous Hall coefficient of Mn_3CuN is positive as can be seen from Fig. 3, while it is negative in Mn_4N. This might be related to the sign change of the anomalous Hall coefficient with Dy composition in $Mn_{4-x}Dy_xN$ films [28]. However, the

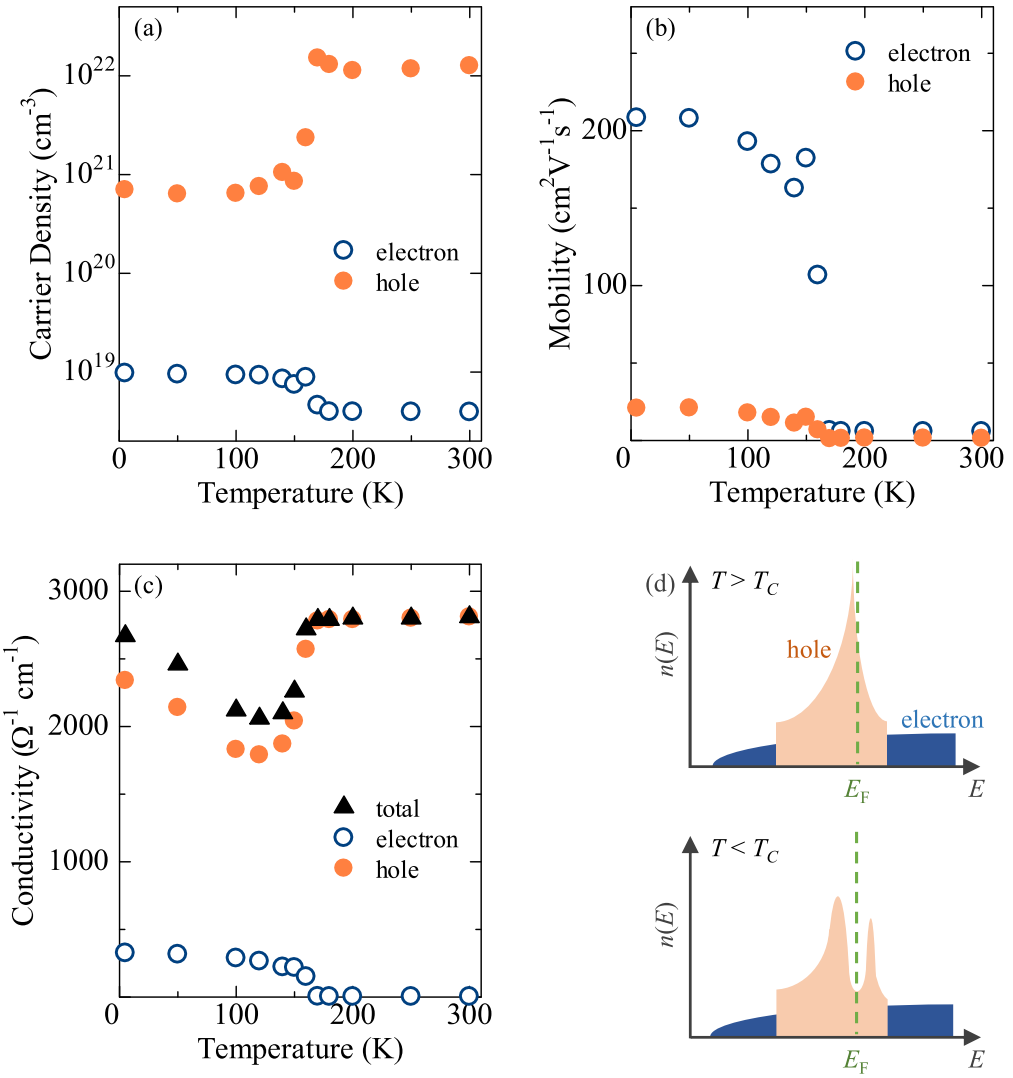

FIG. 4. Temperature dependence of (a) carrier concentration and (b) carrier mobility extracted from the Hall coefficient data. (c) The electrical conductivity calculated from the carrier concentration and mobility plotted in (a) and (b). (d) Schematic illustration of the electronic structure deduced from the Hall resistivity data.

microscopic origin of AHE in Mn_3CuN is beyond the scope of the present paper and requires further study.

Turning our attention to the high-field region of Fig. 3, it is notable that the sign of the slope had changed when the temperature was decreased through the phase transition. Additionally, the field dependence of ρ_H is nonlinear at high fields, suggesting that both electrons and holes are participating in the transport properties. The Hall resistivity is a sum of two contributions, $\rho_H = \rho_{OH} + \rho_{AH}$, where ρ_{OH} and ρ_{AH} represent the ordinal and anomalous Hall resistivities, respectively. On the assumption that ρ_{AH} is saturated at high fields, we fitted the semiclassical, two-carrier model [29] to the ρ_H data in the field range of $\mu_0 H \geqslant 5\,\mathrm{T}$ (μ_0 is the permeability of vacuum) and extracted the electron and hole concentration (n_e and n_h) and mobility (μ_e and μ_h). We also put a constraint on the fitting parameters that they reproduce the resistivity data as well. An example of the fitting is displayed in the inset of Fig. 3, which shows a good agreement with the experimental data.

The extracted carrier concentrations of the two types of carriers, as well as their mobility, are plotted as a function of temperature in Figs. 4(a) and 4(b), respectively. Above T_C, n_h is significantly larger than n_e, which explains naturally the positive slope of the Hall resistivity (Fig. 3). n_h is on the order of $10^{22}\,\mathrm{cm}^{-3}$, which is within the range of a metal. However, as has been pointed out earlier [5,7], $\rho(T)$ of Mn_3CuN has a very weak temperature dependence at $T > T_C$. This can be accounted for by the low mobility of the carriers [Fig. 4(b)]. In the magnetically ordered state at $T < T_C$, the carrier mobility increases, especially that of electrons. This suggests that magnetic scattering is the reason for the low mobility at $T > T_C$, as speculated in earlier studies [9,30].

With lowering the temperature, n_h decreases drastically at T_C, while n_e increases slightly. However, n_h is still larger than n_e at $T < T_C$, despite the negative slope of Hall resistivity (Fig. 3). On the other hand, the electron mobility μ_e increased significantly at lower temperatures. The change to a negative slope of ρ_H at low temperature should therefore be attributed to the increase of μ_e. It is interesting though, that the electronic conductivity is dominated by holes rather than electrons as shown in Fig. 4(c), which plots the hole conductivity ($n_h e \mu_h$, e

denotes the elementary charge), electron conductivity ($n_e e\mu_e$), and their sum calculated from the parameters shown in Figs. 4(a) and 4(b). This is because n_h is still almost two orders of magnitude larger than n_e at $T < T_C$, while the difference between μ_e and μ_h is only an order of magnitude.

According to theoretical consideration about manganese nitrides Mn_3AN in general, Mn d and N p orbitals form narrow subbands near the Fermi level (E_F) that partly overlap a broad conduction band [11,12]. Each of the subbands consists of a bonding and an antibonding band, both having a singularity in the density of states (DOS). Structural instabilities can result from a Jahn-Teller-type effect if E_F locates close to one of these singularities, which has been considered the origin of the structural transition in Mn_3CuN. Although this model has been widely accepted, its validity has not been thoroughly tested by experiments, and the details such as the character of the bands that form the electronic structure near E_F and/or the position of E_F have not been elucidated. Our results indicate that there are two types of carriers, holes are the majority carriers, and n_h decreases drastically at T_C with lowering the temperature. These results can be consistently understood within the framework of the theoretical model if E_F locates slightly above the singularity of the antibonding band. The narrow band with larger DOS would then have a hole character explaining that n_h is large, while the broad conduction band with lower DOS should have an electron character, as schematically drawn in the upper part of Fig. 4(d). The drastic decrease of n_h at T_C is consistent with the opening of an energy gap at E_F accompanying the Jahn-Teller distortion. Hence, our results can be regarded as supporting the theoretical model, and allowed us to locate E_F. It is also interesting to point out that n_h is still larger than n_e at $T < T_C$. This implies that the energy gap is not fully opened, as depicted in the lower part of Fig. 4(d).

IV. SUMMARY

We fabricated epitaxial Mn_3CuN thin films by an ultrahigh-field sputtering method and measured the physical properties. While the as-grown films had rather poor crystallinity, annealing in vacuum with Ti powders had significantly improved the film quality. We found that the Curie temperature is strongly strain dependent by measuring the magnetization of the films grown on different substrates. The carrier concentration and mobility extracted from Hall resistivity data showed that holes are the majority carrier throughout the whole temperature range investigated. The carrier mobility was very small above T_C, probably because of strong magnetic scattering that accounts well for the weak temperature dependence of $\rho(T)$ at $T > T_C$. At T_C, we observed a drastic change in the hole concentration that can be associated with Jahn-Teller distortion. Based on these results, we discussed the electronic structure of the present compound consulting a theoretical model that was derived from a general discussion about manganese nitrides.

ACKNOWLEDGMENTS

This work was partially supported by a Grant-in-Aid for Scientific Research (B) (Grant No. 26286038) and Grant-in-Aid for Challenging Exploratory Research (Grant No. 16K13684) from the Ministry of Education, Culture, Sports, Science and Technology (MEXT) and the Japan Society for the Promotion of Science.

[1] D. Fruchart and E. F. Bertaut, J. Phys. Soc. Jpn. **44**, 781 (1978).
[2] K. Takenaka and H. Takagi, Appl. Phys. Lett. **87**, 261902 (2005).
[3] R. Huang, L. Li, F. Cai, X. Xu, and L. Qian, Appl. Phys. Lett. **93**, 081902 (2008).
[4] J. Yan, Y. Sun, H. Wu, Q. Huang, C. Wang, Z. Shi, S. Deng, K. Shi, H. Lu, and L Chu, Acta. Mater. **74**, 58 (2014).
[5] K. Asano, K. Koyama, and K. Takenaka, Appl. Phys. Lett. **92**, 161909 (2008).
[6] K. Takenaka, T. Shibayama, D. Kasugai, and T. Shimizu, Jpn. J. Appl. Phys. **51**, 08HF05 (2012).
[7] E. O. Chi, W. S. Kim, and N. H. Hur, Solid State Commun. **120**, 307 (2001).
[8] K. Takenaka, A. Ozawa, T. Shibayama, N. Kaneko, T. Oe, and C. Urano, Appl. Phys. Lett. **98**, 022103 (2011).
[9] T. Oe, C. Urano, N. Kaneko, M. Hadano, and K. Takenaka, Appl. Phys. Lett. **103**, 173518 (2013).
[10] D. Matsunami, A. Fujita, K. Takenaka, and M. Kano, Nat. Mater. **14**, 73 (2015).
[11] J. Jardin and J. Labbé, J. Appl. Phys. **52**, 1627 (1981).
[12] J. Jardin and J. Labbé, J. Solid State Chem. **46**, 275 (1983).
[13] M. Aoki, H. Yamane, M. Shimada, and T. Kajiwara, J. Alloys Compd. **364**, 280 (2004).
[14] For a review, see A. E. Clark, in *Ferromagnetic Materials*, Vol. 1, edited by E. P. Wohlfarth (Elsevier, Amsterdam, 1980), pp. 531–589.
[15] A. E. Clark, J. P. Teter, and O. D. McMasters, J. Appl. Phys. **63**, 3910 (1988).
[16] Y. Sun, C. Wang, Y. Na, L. Chu, Y. Wen, and M. Nie, Mater. Res. Bull. **45**, 1230 (2010).
[17] Y. Na, C. Wang, Y. Sun, L. Chu, M. Nie, N. Ji, and J. P. Wang, Mater. Res. Bull. **46**, 1022 (2011).
[18] M. Aoyama, K. Takenaka, and H. Ikuta, J. Alloys Compd. **577**, S314 (2013).
[19] T. Matsuda, S. Kashimoto, A. Imai, Y. Yanagi, Y. Itoh, H. Ikuta, U. Mizutani, K. Sakurai, and H. Hazama, Physica C **392-396**, 696 (2003).
[20] Y. Yanagi, T. Matsuda, H. Hazama, K. Yokouchi, M. Yoshikawa, Y. Itoh, T. Oka, H. Ikuta, and U. Mizutani, Physica C **426-431**, 764 (2005).
[21] K. Takenaka, T. Shibayama, K. Asano, and K. Koyama, J. Phys. Soc. Jpn. **79**, 073706 (2010).
[22] D. Kasugai, A. Ozawa, T. Inagaki, and K. Takenaka, J. Appl. Phys. **111**, 07E314 (2012).
[23] J. C. Lin, B. S. Wang, S. Lin, P. Tong, W. J. Lu, L. Zhang, B. C. Zhao, W. H. Song, and Y. P. Sun, J. Appl. Phys. **111**, 113914 (2012).

[24] N. Nagaosa, J. Sinova, S. Onoda, A. H. MacDonald, and N. P. Ong, Rev. Mod. Phys. **82**, 1539 (2010).
[25] D. Yue and X. Jin, J. Phys. Soc. Jpn. **86**, 011006 (2017).
[26] X. Shen, A. Chikamatsu, K. Shigematsu, Y. Hirose, T. Fukumura, and T. Hasegawa, Appl. Phys. Lett. **105**, 072410 (2014).
[27] M. Meng, S. X. Wu, L. Z. Ren, W. Q. Zhou, Y. J. Wang, G. L. Wang, and S. W. Li, Appl. Phys. Lett. **106**, 032407 (2015).
[28] M. Meng, S. X. Wu, W. Q. Zhou, L. Z. Ren, Y. J. Wang, G. L. Wang, and S. W. Li, J. Appl. Phys. **118**, 053911 (2015).
[29] J. M. Ziman, *Principles of the Theory of Solids*, 2nd ed. (Cambridge University Press, Cambridge, 1972).
[30] M. Hadano, A. Ozawa, K. Takenaka, N. Kaneko, T. Oe, and C. Urano, J. Appl. Phys. **111**, 07E120 (2012).